The Astrophysical Journal, 773:51 (9pp), 2013 August 10 doi:10.1088/0004-637X/773/1/51

REFLECTION-DOMINATED NUCLEAR X-RAY EMISSION IN THE EARLY-TYPE GALAXY ESO 565–G019

P. Gandhi[1,2], Y. Terashima[3], S. Yamada[4], R. F. Mushotzky[5], Y. Ueda[6], W. H. Baumgartner[7], D. M. Alexander[2], J. Malzac[8,9], K. Vaghmare[10], T. Takahashi[1,11], and C. Done[2]

[1] Institute of Space and Astronautical Science (ISAS), Japan Aerospace Exploration Agency, 3-1-1 Yoshinodai, Chuo-ku, Sagamihara, Kanagawa 252-5210, Japan
[2] Department of Physics, Durham University, Durham DH1-3LE, UK
[3] Department of Physics, Ehime University, 2-5 Bunkyo-cho, Matsuyama, Ehime 790-8577, Japan
[4] Cosmic Radiation Laboratory, Institute of Physical and Chemical Research (RIKEN), Wako, Saitama 351-0198, Japan
[5] Department of Astronomy, University of Maryland College Park, College Park, MD 20742, USA
[6] Department of Astronomy, Kyoto University, Kitashirakawa-Oiwake-cho, Sakyo-ku, Kyoto 606-8502, Japan
[7] NASA/Goddard Space Flight Center, Astrophysics Science Division, Greenbelt, MD 20771, USA
[8] Université de Toulouse, UPS-OMP, IRAP, F-31028 Toulouse, France
[9] CNRS, IRAP, 9 Ave. Colonel Roche, BP 44346, F-31028 Toulouse Cedex 4, France
[10] IUCAA, Post Bag 4, Ganeshkhind, Pune 411007, India
[11] Department of Physics, University of Tokyo, 7-3-1 Hongo, Bunkyo, Tokyo 113-0033, Japan
Received 2013 February 11; accepted 2013 May 21; published 2013 July 25

ABSTRACT

We present the discovery of a reflection-dominated active galactic nucleus (AGN) in the early-type radio-quiet galaxy ESO 565–G019 with *Suzaku* and *Swift*/Burst Alert Telescope. The source X-ray spectrum below 10 keV is characteristic of other Compton-thick (CT) AGNs, clearly showing an inverted continuum and prodigious fluorescence iron emission above ∼3 keV. A Compton shoulder to the neutral Fe Kα line also appears to be present. There is evidence for long-term hard X-ray flux variability that we associate with changes in the intrinsic AGN power law. More of such reflection-dominated AGNs should be uncovered in the near future with the increased sensitivity of ongoing and new hard X-ray surveys. ESO 565–G019 is hosted in an early-type galaxy whose morphology has been variously classified as either type E or type S0. Only about 20 bona fide CT-AGNs have been identified in the local universe so far, and all exist in host galaxies with late Hubble types (S0 or later). CT columns of nuclear obscuring gas are uncommon in early-type galaxies in the local universe, so confirmation of the exact morphological class of ESO 565–G019 is important. Infrared photometry also shows the presence of large quantities of cool dust in the host, indicative of significant ongoing star formation. ESO 565–G019 may be the first identified local example of minor-merger-driven CT-AGN growth in an early-type host, or may be the result of interaction with its neighboring galaxy ESO 565–G018 in a wide pair.

Key words: galaxies: active – X-rays: galaxies – X-rays: individual (ESO 565–G019, ESO 565–G018)

Online-only material: color figures

1. INTRODUCTION

The spectrum of the cosmic hard X-ray background requires a substantial contribution from heavily obscured active galactic nuclei (AGNs; e.g., Setti & Woltjer 1989; Fabian & Iwasawa 1999; Gandhi & Fabian 2003; Gilli et al. 2007; Treister et al. 2009; Ballantyne et al. 2011; Brightman & Ueda 2012; Akylas et al. 2012). Extensive searches have been carried out for the most obscured population of objects using a range of multi-wavelength selection techniques (e.g., Bassani et al. 1999; Risaliti et al. 1999; Gandhi et al. 2004; Guainazzi et al. 2005; Martínez-Sansigre et al. 2007; Fiore et al. 2008; Goulding & Alexander 2009; Alexander et al. 2011; Severgnini et al. 2012 and references therein).

Each technique suffers from some form of incompleteness. In particular, Compton-thick (CT) AGNs with equivalent neutral hydrogen column densities of obscuring gas $N_{\rm H} \gtrsim 1.2$–1.5×10^{24} cm^{-2} are notoriously difficult to identify, even in the local universe. Their X-ray spectra are expected to peak in the hard X-ray regime above 10 keV (e.g., Matt et al. 2000), but Compton downscattering can significantly attenuate even hard X-rays. X-rays from nuclear stellar activity or from the AGN component scattered into the line of sight (los) can then overwhelm obscured AGN signatures.

Here, we present high-quality *Suzaku* follow-up of a galaxy selected based upon its hard X-ray properties from the 70 month *Swift* Burst Alert Telescope (BAT) sky survey (Baumgartner et al. 2013). ESO 565–G019 is generally classified as optical morphological type E,[12] hosting an optically classified Seyfert 2 (Véron-Cetty & Véron 2006). No pointed X-ray observations below 10 keV have been published. Its detection in the *Swift*/BAT survey at higher energies suggests that the source may have been previously overlooked. We find a reflection-dominated (RD) X-ray continuum and strong Fe fluorescence emission lines, and show that the AGN is likely to be hidden by CT columns of obscuring gas. CT-AGN activity in early-type galaxies is relatively uncommon in the local universe, and we discuss how ESO 565–G019 fits into this context.

Luminosities are based on a redshift $z = 0.017379$ (72.4 Mpc) corrected to the reference frame of the cosmic microwave background for $H_0 = 73$ km s^{-1} Mpc^{-1}, $\Omega_{\rm M} = 0.27$, and $\Omega_\Lambda = 0.73$.[13]

2. OBSERVATIONS

2.1. *Swift*/BAT

The BAT instrument on board the *Swift* mission (Gehrels et al. 2004; Barthelmy et al. 2005) has been used to compile the 70 month hard X-ray catalog (Baumgartner et al. 2013; see

[12] http://leda.univ-lyon1.fr/
[13] http://ned.ipac.caltech.edu

also http://heasarc.gsfc.nasa.gov/docs/swift/results/bs70mon) including publicly released spectra and diagonal response matrices, which we use here. The effective source exposure is 8.1 Ms. The source displays a relatively flat power-law photon index of $\Gamma = 1.37^{+0.39}_{-0.40}$ and 14–195 keV flux of $2.1(\pm0.6) \times 10^{-11}$ erg s^{-1} cm^{-2}. The corresponding luminosity is 1.4×10^{43} erg s^{-1}.

2.2. *Suzaku*

ESO 565–G019 was observed with *Suzaku* (Mitsuda et al. 2007) starting on 2012 May 20 for an on-source effective time of 78.9 ks (ObsID = 707013010). Both instruments, the X-ray Imaging Spectrometer (XIS; Koyama et al. 2007) and the Hard X-ray Detector (HXD; Takahashi et al. 2007; Kokubun et al. 2007), were operated in standard mode with XIS-nominal pointing.

Data reduction and processing were performed using the *Suzaku* software version 18, FTOOLS v6.12 (Blackburn 1995). Standard recommended event selection criteria[14] were employed using XSELECT v2.4b. The net XIS and HXD good times were 62.9 and 66.5 ks, respectively.

XIS (sensitive below 10 keV) counts were integrated within a circular aperture of radius 3.′4 and background counts extracted from source-free regions. ESO 565–G019 is by far the brightest source within the XIS field of view (fov). A polygonal background aperture was constructed to sample large parts of the background over the remaining fov, free from contamination by other possible faint sources. The latest version of the calibration database v20120902 was used for generating response matrices and auxiliary response files.

For HXD, data from the PIN diodes below ∼60 keV were extracted using the FTOOL `hxdpinxbpi`, which returns the dead-time-corrected source spectrum and a background spectrum based upon the "tuned" background model provided by the *Suzaku* team. Below ∼30 keV, this model was found to severely overestimate the earth-occultation background data,[15] which were also extracted for comparison. This is a result of insufficient samples for good model reconstruction of the long-term background trend during 2012 mid-May, and the model was discarded in favor of the earth-occultation data. The contribution of the cosmic X-ray background (CXB) component was simulated in a standard manner[16] and added to the earth-occultation spectrum. For model fitting using χ^2 minimization, spectral counts were grouped to obtain a minimum significance of 4 bin^{-1}. At higher energies, the source is faint enough that data from the scintillator array (gadolinium silicate) were ignored.

3. X-RAY FITTING

For modeling the broadband data, the soft emission below 2 keV was parameterized with a hot thermal plasma APEC component (Smith et al. 2001), although alternatives are discussed in Section 5.1. The underlying continuum component is an absorbed intrinsic power law (hereafter IPL) with photon index $\Gamma_{\rm IPL}$. Furthermore, a fraction ($f_{\rm SPL}$) of the IPL scattered into the los (hereafter SPL) from an optically thin medium was found to be necessary. Emission lines were modeled as Gaussian profiles at a fixed systemic redshift $z = 0.016285$.[17] Fixed Galactic $N_{\rm H} = 4.1 \times 10^{20}$ cm^{-2} was also included, based upon H I measurements along the los (Dickey & Lockman 1990). The two front-illuminated (fi) CCDs XIS0 and 3 were combined for fitting, and the energy ranges of 1.7–1.9 and 2.1–2.3 keV were ignored due to instrumental calibration uncertainties related to Si and Au edges. All spectral fitting was carried out using XSPEC v12.8 (Arnaud 1996) and uncertainties are quoted at the 90% level.

3.1. Absorbed Power Law Plus PEXRAV: Model P

We next added in a PEXRAV (Magdziarz & Zdziarski 1995) component characterizing "pure reflection" (i.e., negative-valued model parameter R in XSPEC terminology). The reflected component was taken to be unabsorbed, while photoelectric absorption (`phabs`) and Compton downscattering (`cabs`; including Klein–Nishina corrections at high energies) due to a single heavy obscurer were introduced for the IPL. This model is referred to as model P. HXD data cross-normalization was fixed at 1.16 relative to fi,[18] while that for the back-illuminated CCD was left free.

3.2. MYTORUS: Model M

The PEXRAV model assumes reflection off a slab with infinite optical depth. More sophisticated treatment of reflection, including a classical circumnuclear torus geometry and self-consistent inclusion of fluorescence emission, was carried out with the MYTORUS model (Yaqoob 2012). All "minimal" table model components were included. These comprise (1) the distortion of the zeroth-order continuum due to obscuration by the torus, (2) Compton scattering off gas in the torus (MYTORUSS), and (3) associated fluorescence line emission (MYTORUSL). The normalizations of these three components were tied to that of IPL. MYTORUS assumes no high-energy cutoff up to a termination energy of 500 keV, and has precomputed table model grids for $N_{\rm H}$ up to 10^{25} cm^{-2}. Fe Kβ (7.06 keV) is included by default in the model, reducing the significance of Fe XXVI. MYTORUS allows decoupling the los obscuring column ($N_{\rm H}$(los)) from that responsible for the scattered continuum and fluorescence ($N_{\rm H}$(scatt)). This model is referred to as model M.

3.3. Accounting for Long-term Variability

As we will discuss in detail later, the *Suzaku*/HXD data show a higher hard X-ray flux level than *Swift*/BAT. Under the assumption that variability is dominated by the power law, we introduced a further cross-normalization constant (CONST$_{\rm IPL}$) in both models P and M to account for different intrinsic (i.e., IPL) source fluxes measured by *Suzaku* and *Swift*. In this scenario, the absolute flux of the reflection and scattered components do not vary, with their normalizations being tied to the same value as the IPL between all instruments. The XIS regime, being reflection-dominated, is not greatly sensitive to changes in the IPL, though it is treated self-consistently throughout.

4. RESULTS

The *Suzaku* XIS spectra are shown in Figure 1. A flat continuum above 2 keV and prominent emission due to Fe fluorescence are seen. Characterizing the XIS spectrum with an absorbed IPL alone results in an extremely flat $\Gamma^{\rm XIS}_{\rm IPL} = 0.6^{+0.5}_{-0.4}$, but with an unacceptable goodness-of-fit statistic. These properties clearly

[14] http://heasarc.gsfc.nasa.gov/docs/suzaku/analysis/abc
[15] Selected using events with ELV < -5; effective exposure time 41.7 ks.
[16] http://heasarc.gsfc.nasa.gov/docs/suzaku/analysis/abc
[17] http://ned.ipac.caltech.edu
[18] http://heasarc.gsfc.nasa.gov/docs/suzaku/analysis/abc/node8.html#SECTION00872000000000000000

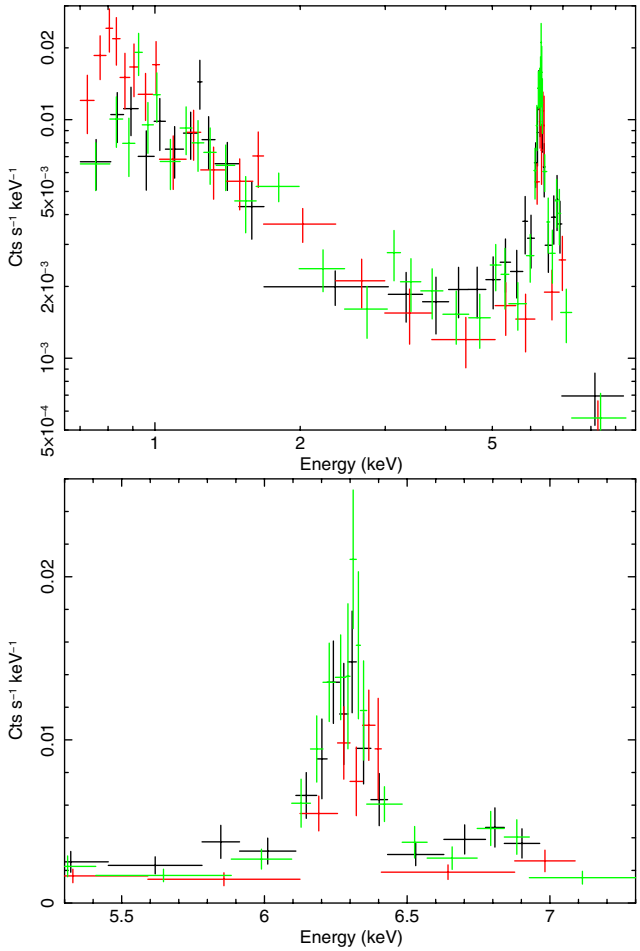

Figure 1. Top: data for XIS0, 1, and 3 are shown in black, red, and green, respectively. Bottom: zoomed-in Fe line region shown on a linear scale.
(A color version of this figure is available in the online journal.)

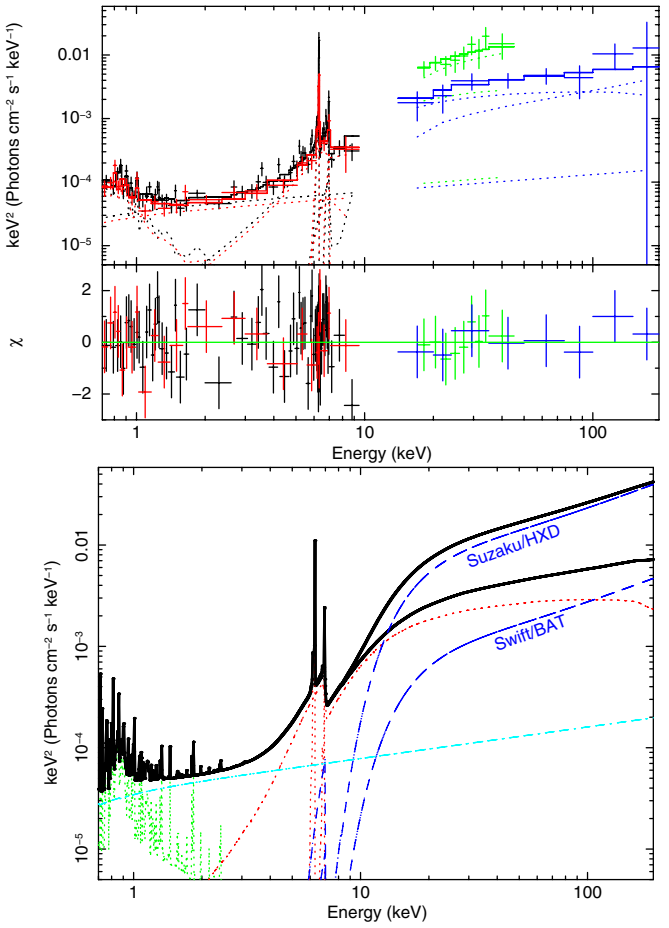

Figure 2. Top: best-fitting unfolded model M and data for front-illuminated (XIS0+3) CCDs shown in black and back-illuminated XIS1 shown in red, while those for HXD/PIN and BAT are shown in green and blue, respectively. Bottom: corresponding model components IPL (blue dashed), MYTORUSS + MYTORUSL (red dotted), SPL (cyan dash-dotted), and APEC (green dotted).
(A color version of this figure is available in the online journal.)

imply the presence of heavy obscuring and reflecting matter in the source.

With regard to the broadband fits using models P and M, acceptable fits were found in both cases with the parameters reported in Table 1. The determined los $N_{\rm H}$ and its confidence limits lie well above 10^{24} cm^{-2}, implying CT obscuration. In model M, $N_{\rm H}$(los) is larger than $N_{\rm H}$(scatt). The underlying power law appears to show clear variability between *Suzaku* and *Swift*, characterized by CONST$_{\rm IPL}$. The IPL high-energy cutoff ($E_{\rm cutoff}$) remains unconstrained and was fixed at 500 keV in model P. The inclination angle of the reflector (θ) was left free and is also unconstrained.

The equivalent width (EW) of Fe Kα on the observed continuum is $\sim$1.1 keV. At least one additional emission line is required, with centroid energy close to that of redshifted Fe XXVI (6.97 keV) and EW(Fe XXVI) $\approx$ 0.3 keV. Adding a third Fe line (e.g., due to Fe Kβ) does not provide a significant improvement.

The resultant fits of the two models (Table 1) show that model M is marginally better than model P, though both are acceptable statistically. The unfolded model M is shown in Figure 2.

5. DISCUSSION

Using *Suzaku*, we have carried out the first pointed X-ray study of ESO 565–G019. In this section, we discuss some salient points of our analysis.

5.1. X-Ray Spectrum below 10 keV

The soft band below about 2 keV has been modeled with contributions from a hot interstellar thermal plasma and the SPL, which has a scattering fraction ($f_{\rm SPL}$) of a few percent, as has been inferred from modeling low spectral resolution (CCD) data of Seyfert galaxies (e.g., Turner et al. 1997; Cappi et al. 2006). Early-type galaxy halos and sources dominated by starburst activity typically show thermal emission from diffuse plasma with temperatures of $\lesssim$1 keV (e.g., Forman et al. 1985; Done et al. 2003; Konami et al. 2012). On the other hand, high-resolution grating spectra of bright nearby Seyferts, including other CT-AGNs, have instead shown that the soft X-ray regime may be dominated by emission from gas photoionized by the nucleus (e.g., Sako et al. 2000; Kinkhabwala et al. 2002; Iwasawa et al. 2003; Armentrout et al. 2007; Guainazzi & Bianchi 2007). Distinguishing between these various scenarios will require higher spectral resolution data than we possess at present, which should be possible using the micro-calorimeter on board *Astro-H* (Takahashi et al. 2012).

With regard to the SPL, the luminosity in this component is $\sim 10^{41}$ erg s^{-1}. This is low enough that some part of the scattered emission may arise as the integrated emission from point sources other than the AGN within ESO 565–G019 (e.g., X-ray binaries). *Suzaku* is unable to disentangle this

Table 1
XSPEC Fits to the X-Ray Spectrum of ESO 565–G019

Component	Parameters	AGN Model P[a] (PEXRAV)	AGN Model M[a] (MYTORUS)	Units
APEC	kT	$0.69^{+0.07}_{-0.10}$	0.67 ± 0.09	keV
	Abundance	$0.14^{+u}_{-0.18}$	0.3[b]	
	Norm	$15.3^{+18.9}_{-9.1}$	7.6 ± 1.6	$\times 10^{-5}$[c]
	$F^{\rm obs}_{0.5-2}$	$1.42^{+0.03}_{-0.36}$	$1.44^{+0.03}_{-0.46}$	$\times 10^{-13}$ erg s^{-1} cm^{-2}
	$L^{\rm APEC}_{0.5-2}$ [d]	6.3	5.0	$\times 10^{40}$ erg s^{-1}
AGN Continuum	$N_{\rm H}$(los)	$2.1^{+1.5}_{-0.5}$	$4.4^{+u}_{-1.5}$	$\times 10^{24}$ cm^{-2}
	$N_{\rm H}$(scatt)	...	$1.0^{+1.3}_{-0.4}$	$\times 10^{24}$ cm^{-2}
	$\Gamma_{\rm IPL}$	$1.69^{+0.31}_{-0.29}$	$1.72^{+0.41}_{-0.27}$	
	θ	81^{+u}_{-u}	67^{+14}_{-42}	deg
	$E_{\rm cutoff}$	500[b]	...	keV
	Norm$_{\rm IPL}$	$2.8^{+28}_{-2.6}$	$4.2^{+14}_{-2.2}$	$\times 10^{-3}$ ph s^{-1} cm^{-2} keV^{-1}
	$\Gamma_{\rm SPL}$	$=\Gamma_{\rm IPL}$	$=\Gamma_{\rm IPL}$	
	$F^{\rm obs}_{2-10}$	6.5^{+10}_{-4}	7.1 ± 0.8	$\times 10^{-13}$ erg s^{-1} cm^{-2}
	$L^{\rm IPL}_{\rm XIS(2-10)}$ [d]	3.3	6.2	$\times 10^{43}$ erg s^{-1}
	$L^{\rm IPL}_{\rm BAT\ (14-195)}$ [d]	2.5	3.4	$\times 10^{43}$ erg s^{-1}
	$L^{\rm IPL}_{\rm HXD\ (10-100)}$ [d]	8.6	15.3	$\times 10^{43}$ erg s^{-1}
	CONST$_{\rm IPL}$[e]	$4.6^{+52}_{-2.2}$	$6.0^{+127}_{-2.7}$	
	$L^{\rm IPL}_{2-10}$ [d]	0.7	1.0	$\times 10^{43}$ erg s^{-1}
	R	$-0.9^{+1.9}_{-u}$	...	
	$f_{\rm SPL}$	$1.0^{+35}_{-0.9}$	$0.9^{+0.6}_{-0.7}$	$\times 10^{-2}$
Lines	$E_{\rm obs}$	6.28 ± 0.01	...	keV
	σ	0.001[b]	[f]	keV
	Norm	1.09 ± 0.12		$\times 10^{-5}$ ph s^{-1} cm^{-2}
	EW	1.1 ± 0.6	1.2	keV
	$E_{\rm rest}$	6.38 ± 0.01	[f]	keV
	$\Rightarrow$ ID = Fe Kα			
	$E_{\rm obs}$	6.84 ± 0.07	...	keV
	σ	0.001[b]	...	keV
	Norm	2.1 ± 1.2	...	$\times 10^{-6}$ ph s^{-1} cm^{-2}
	EW	$0.20^{+0.20}_{-0.17}$	...	keV
	$E_{\rm rest}$	6.95 ± 0.07	...	keV
	$\Rightarrow$ ID = Fe XXVI			
	EW$_{\rm K\beta}$	...	0.2	keV
χ^2/dof		96/103	95/108	

Notes. u: unconstrained.
[a] Model P: CONST * PHABS[$\mapsto$ $N_{\rm H}^{\rm Gal}$](APEC + PEXRAV + PHABS*CABS*CONST$_{\rm IPL}$*POW[$\mapsto$IPL] + CONST[$\mapsto$ $f_{\rm SPL}$]*POW[$\mapsto$IPL] + GAUSS($\times$2)). Model M: CONST * PHABS[$\mapsto$ $N_{\rm H}^{\rm Gal}$](APEC + (*ETABLE{`mytorus_Ezero_v00.fits`}*CONST$_{\rm IPL}$*POW[$\mapsto$IPL] + ATABLE{`mytorus_scatteredH500_v00.fits`} + ATABLE{`mytl_V000010nEp000H500_v00.fits`} +CONST[$\mapsto$ $f_{\rm SPL}$]*POW[$\mapsto$IPL]). In both models, the first CONST refers to the instrumental cross-normalization. Galactic absorption $N_{\rm H}^{\rm Gal}$ is fixed to 4.06×10^{20} cm^{-2}. The normalizations for the table components are tied to IPL.
[b] fixed.
[c] APEC norm quoted in units of 10^{14} cm^{-5}.
[d] Absorption-corrected luminosities for the APEC and AGN components are quoted after setting all other model components to zero. L_{2-10} is to be regarded as the long-term 2–10 keV IPL power and is equal to $L_{\rm XIS\ (2-10)}$/CONST$_{\rm IPL}$.
[e] HXD IPL normalization relative to BAT.
[f] Fluorescence in MYTORUS model includes Fe Kα and Kβ assuming no velocity shift. A smoothing width of σ = 1 eV was assumed.

component spatially, but this should be possible with the *Chandra* satellite.

Over the 4–10 keV regime, the observed emission is found to be reflection-dominated. With its high $N_{\rm H}$(los) and strong Fe line, ESO 565–G019 joins the ranks of well-known local CT-AGNs with strong Fe lines such as NGC 1068 (see, e.g., the compilation by Levenson et al. 2002).

The variability observed between HXD and BAT above 10 keV (discussed further in Section 5.3) also has consequences for the lower energy range. It is important to remember that

we have assumed the variability to be dominated by the IPL normalization alone, and that the absolute fluxes of the reflection and scattering components do not change because they ought to respond on long time spans. This means that any fit variables defined relative to the IPL (i.e., $f_{\rm SPL}$, R) also change depending upon the data set considered. Table 1 states values relative to the long-term IPL flux probed by *Swift*/BAT. So when considering the values of these variables in the *Suzaku* data alone, these will effectively be lower by a factor of CONST$_{\rm IPL}$. Similarly, in Table 1, we have distinguished between the absorption-corrected IPL luminosities $L_{\rm XIS\ (2-10)}$ and L_{2-10}. $L_{\rm XIS\ (2-10)}$ is the absorption-corrected 2–10 keV luminosity for the XIS consistent with the HXD flux level (the two instruments observed the source simultaneously on the same date). On the other hand, L_{2-10} is lower by a factor of CONST$_{\rm IPL}$ and may be considered the long-term average 2–10 keV IPL luminosity based upon the *Suzaku*/XIS and *Swift*/BAT data sets. These variables are collected and tabulated together with CONST$_{\rm IPL}$ in Table 1.

The inferred long-term absorption-corrected IPL luminosity for models P and M ranges over $L_{2-10} \sim (0.7–1) \times 10^{43}$ erg s^{-1}. Mean X-ray bolometric corrections and Eddington fractions of the *Swift*/BAT AGN sample have been studied by Vasudevan et al. (2010), who showed that this sample has a comparatively low Eddington ratio distribution overall (Vasudevan et al. 2010). For a typical bolometric correction ($L_{\rm Bol}$:L_{2-10}) $\sim$ 10–30, the mean $L_{\rm Bol}$ of ESO 565–G019 lies within the range of $\sim(0.7–3) \times 10^{44}$ erg s^{-1}. If the accretion luminosity of the source is 10% of the Eddington value on average, then this would imply a supermassive black hole mass range of (0.5–2) $\times$ 10^7 $M_\odot$.

5.2. Fe Complex

The Fe Kα line is strong, with EW(Fe Kα) in excess of 1 keV with respect to the observed continuum. With respect to the reflection continuum alone, we find EW(Fe Kα) $\approx$ 1.8 keV (model P) and 1.4 keV (model M). Fe line fluorescence can, in principle, constrain the geometry of the reflecting matter. The observed range of EWs is certainly consistent with the line and reflection continuum originating in the same location, presumably the torus (Matt et al. 1996). With regard to the inclination angle of the reflector, Table 1 suggests highly inclined θ values. In the parameter space of torus reflection models (e.g., Matt et al. 1996; Levenson et al. 2002), higher inclinations favor larger Fe line EWs, qualitatively consistent with our findings. However, we stress that uncertainties on θ are not negligible, and this parameter remains unconstrained in model P.

Downscattering of emission line photons also results in a characteristic hump known as the Compton shoulder (CS) redward of the rest-frame line centroid. The strength of this feature can be a sensitive diagnostic of the column density (Matt 2002). CS signatures have been found in several CT-AGNs studied by *Suzaku* (e.g., Itoh et al. 2008; Awaki et al. 2008). A single downscattering results in a maximum energy decrement of $\approx$160 eV, which is close to the spectral resolution of the XIS CCDs. In fact, Table 1 shows that the rest-frame energy of the Fe Kα line in ESO 565–G019 measured using a Gaussian profile in model P is slightly lower than the expected value of 6.4 keV, which is likely to be caused by a CS blended with the line.

A CS is included self-consistently within model M through MYTORUS. In order to independently check for its existence, we added a CS component to model P, parameterizing it using `xsgacp` (Madejski et al. 2006; Illarionov et al. 1979). We fixed the electron temperature of the scattering medium to a nominal value of 1 eV, and the initial line energy to rest frame 6.40 keV. This resulted in a decrease of $\chi^2 \sim 2$ for the same number of degrees of freedom as in Table 1 (as the neutral Kα line energy is now fixed). The CS component contains a fraction $0.28^{+0.28}_{-0.22}$ of the narrow line photons. The detection of the CS is significant and consistent with the expectation of $\sim$0.2 for reflection from CT material (Matt 2002), though uncertainties are large.

5.3. Hard X-Ray Spectrum and Long-term Variability

Fitting over the full energy range available with *Suzaku*/XIS and *Swift*/BAT suggests that the IPL dominates above $\sim$100 keV in the BAT band, and $E_{\rm cutoff}$ should lie beyond the BAT energy sensitivity range. The fitted $\Gamma_{\rm IPL}$ values are consistent with the median of the distribution of hard X-ray photon indices for radio-quiet Seyferts (Dadina 2008).

$N_{\rm H}$(los) is found to be larger than $N_{\rm H}$(scatt) in model M, which may be a result of clumpiness in the absorber, as supported by a wide range of observational and theoretical work on AGN tori in general (e.g., Hoenig 2013 and references therein). However, with the IPL dominating only in the two highest energy BAT bins, these data do not probe the underlying continuum in detail. This is an important limitation of RD spectra, and leads to various degeneracies (e.g., $N_{\rm H}$(los) being unconstrained at the high end; large uncertainties on CONST$_{\rm IPL}$), and an even more RD hard-band spectrum cannot be ruled out.

The observed *Suzaku*/HXD flux ($F_{15-40\,\rm keV} \approx 1.4 \times 10^{-11}$ erg s^{-1} cm^{-2}) lies above that seen in *Swift*/BAT by a factor of $\approx$3–4 over the same energy range. Systematic uncertainties are important when accounting for the HXD/PIN background reproducibility. Typical earth-occultation data systematic errors are $\sim$3.8%.[19] Including an increased PIN background at this level reduces the HXD excess with respect to BAT to a factor $\sim$2.

These differences cannot be caused by confusion and contamination of the HXD data because the nearest neighbor in the BAT 70 month catalog is PKS 0921–213 at a distance of 2.°6, well outside the collimated $\sim$34′-sized PIN fov.

The BAT data represent a long-term average of the source flux between 2004 December and 2010 September. *Suzaku* observations were carried out 20 months later, so hard X-ray variability may explain the difference. Reflection and scattering are generally thought to occur on $\sim$pc-scale toroidal clouds. Rapid variations are naturally associated with the IPL (as we have modeled). The lower limit of the IPL variation in this scenario is at least a factor of $\sim$2.

It should be noted that we cannot completely rule out strong variations of the hard-band Compton hump originating in an inner disk reflection component (e.g., due to light bending). This possibility can be tested in follow-up X-ray monitoring to search for rapid changes in the reflection continuum and Fe line.

5.4. Multi-wavelength Comparisons

ESO 565–G019 has not been followed up in detail at any wavelength previously, but it has been covered in all-sky surveys in the mid-infrared (MIR), a regime that can provide efficient selection of highly obscured AGNs. For example, the study of Severgnini et al. (2012) finds an MIR number density of

[19] http://heasarc.gsfc.nasa.gov/docs/astroe/prop_tools/suzaku_td/node12.html#SECTION00125110000000000000

CT-AGNs that is two to four times higher than present hard X-ray surveys, though some correction for IR star formation contamination is necessary.

The *Akari* satellite carried out an all-sky survey in 2006–2007 in multiple mid- and far-infrared bands (Ishihara et al. 2010 and references therein). The reported fluxes of ESO 565–G019 at 9 and 90 μm are 77 $\pm$ 13 mJy and 2.90 $\pm$ 0.11 Jy, respectively. Combining these with the observed BAT luminosity, we find that ESO 565–G019 lies close to other CT sources NGC 6240 and NGC 5728 in the MIR:hard-X-ray "color–color" plot of Matsuta et al. (2012, their Figure 5), but not significantly different from the overall distribution of Seyfert colors. This relatively high 90:9 μm flux ratio suggests the presence of large quantities of cool dust, which is well known for NGC 6240 and NGC 5728 (e.g., Rieke et al. 1985; Schommer et al. 1988) but atypical for an early-type galaxy such as ESO 565–G019 (this is discussed further in Section 5.6).

The observed (absorbed) 2–10 keV X-ray luminosity in the *Suzaku* data is $L_{2-10} \sim 4 \times 10^{41}$ erg s^{-1}, and the modeled absorption-corrected power is one to two orders of magnitude higher depending upon which data set is considered. X-ray modeling of CT-AGNs can be highly sensitive to the geometry of the absorber and reflector when the underlying continuum cannot be probed clearly (e.g., Yaqoob 2012). It is thus useful to compare against other diagnostics of the intrinsic power as an independent check of the appropriateness of the X-ray modeling.

Few emission line spectroscopic measurements of the source have been published. Considering photometric data, it has been shown that there is a close correlation between the monochromatic 12 μm continuum torus luminosity and intrinsic 2–10 keV power for local Seyferts (e.g., Horst et al. 2008; Asmus et al. 2011). The best constraints come from isolating the torus spatially in high angular resolution imaging, but such data are not available for ESO 565–G019. The source is detected in the *Wide-field Infrared Survey Explorer* (*WISE*) all-sky survey[20] (Wright et al. 2010). Its W3-band (12 μm) flux is $F(\mathrm{W3}) = 96 \pm 11$ mJy or $\lambda L_{\lambda}(\mathrm{W3}) = 1.6 \times 10^{43}$ erg s^{-1}. Using Equation (2) from Gandhi et al. (2009) then implies $L_{2-10}^{\mathrm{predicted}} = 1.1(\pm 0.2) \times 10^{43}$ erg s^{-1}. This is smaller than the instantaneous IPL power $L_{\mathrm{XIS\ (2-10)}}$ measured in the XIS, but closely matches the inferred long-term intrinsic power estimates L_{2-10} (Table 1). The close match is encouraging because it is the long-term power that is relevant from the point of view of a pc-scale dust torus. Still, we caution that this is an approximate cross-check only because various caveats are unaccounted for (e.g., *WISE* cannot resolve the nucleus with its nominal 6.″5 beam, and the W3 bandpass is broad enough to be affected by various emission and absorption features). In addition, low-level anisotropy in the MIR emission is expected in clumpy torus models (e.g., Hönig et al. 2011). Broadband data that have better direct sensitivity to the IPL will allow more detailed multi-wavelength comparisons.

5.5. Implications for Future Surveys

Present estimates of the contribution of CT-AGNs to the CXB flux are of the order of 10%, with the largest uncertainty being the prevalence of RD sources (e.g., Treister et al. 2009). A wide range of RD-AGN contributions are allowed in principle (Gandhi et al. 2007). At the flux levels probed by current hard X-ray missions, only a tiny fraction of the hard CXB is resolved into point sources, while CT-AGNs are inferred to constitute ~10%–20% of the overall AGN number density (e.g., Sazonov et al. 2007; Burlon et al. 2011; Ricci et al. 2011; Vasudevan et al. 2013).

[20] http://wise2.ipac.caltech.edu/docs/release/allsky/

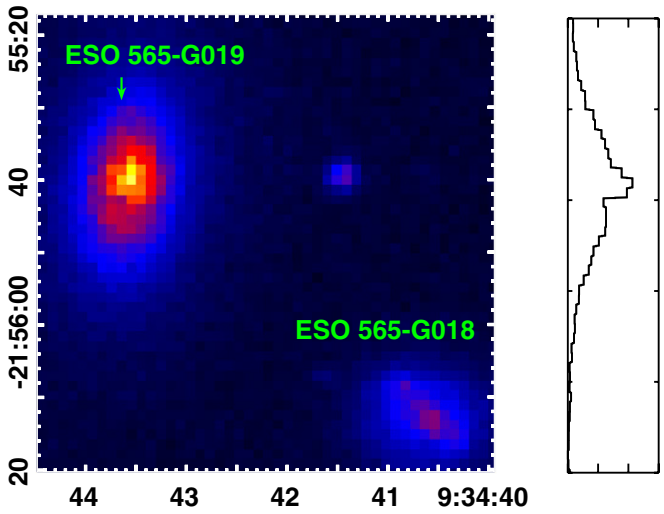

Figure 3. Archival *R*-band image from the ESO-LV catalog of galaxies (archive.eso.org/wdb/astrocat/esolv.html). The core of ESO 565–G019 appears asymmetric, with a slight excess skewed to the north and an apparent flux deficit to its southeast. This is best seen in the vertical profile cut on the right, drawn through the image pixel column containing the arrow. Linear color scaling has been used.

(A color version of this figure is available in the online journal.)

ESO 565–G019 was detected in the BAT 39 month catalog, but not the earlier ones (Cusumano et al. 2010; Tueller et al. 2010). Thus, our work suggests that other RD-AGNs are waiting to be uncovered by hard X-ray selection at fainter fluxes. The new generation of hard X-ray focusing missions *NuSTAR* and *Astro-H* will obtain detailed hard-band spectra of sources like ESO 565–G019 and test the cosmological significance of this population (Ballantyne et al. 2011; Takahashi et al. 2012).

5.6. CT-AGN in an Early-type Galaxy

The host galaxy morphology of ESO 565–G019 was first classified as type E in the ESO/Uppsala survey by Lauberts (1982). A digitized image from this survey is shown in Figure 3. The Third Reference Catalog of Bright Galaxies (RC3) also reported the same classification, but with an extra "?" flag indicating doubt (de Vaucouleurs et al. 1991). The most recent report, based upon a by-eye classification of Digitized Sky Survey plates, is of type S0 (Huchra et al. 2012). Diffraction-limited optical imaging with modern telescopes has not been carried out for this object. Seeing-limited CCD imaging has been analyzed by Prugniel & Heraudeau (1998) and Alonso et al. (2003). Through profile fitting, Prugniel & Heraudeau (1998) find a Sérsic index $n = 3.0$, suggesting that this source is unlikely to host a pseudo-bulge that typically has $n \lesssim 2$ (see the discussion and references in Section 3.1 of Vaghmare et al. 2013). Alonso et al. (2003) obtain an excellent fit by decomposing the total galaxy light profile into a bulge-dominated system plus a disk, with a bulge/disk ratio of 2.56, a typical value for their sample of early-type galaxies. In summary, the host is known to be an early-type bulge-dominated system, but the exact classification remains uncertain.

Only about 20 bona fide CT-AGNs have been identified and studied in detail in the local universe. They are typically radio-quiet systems hosted in spiral galaxies, with only a

handful hosted in galaxies with Hubble types S0,[21] and none in type E (see, e.g., Table 1 of Goulding et al. 2012 and the compilation of Della Ceca et al. 2008). LINERs are invariably X-ray faint, precluding secure CT classification. In the distant universe, morphological classification is more difficult. Based upon the *Hubble Space Telescope* imaging of distant AGN hosts presented in Gabor et al. (2009), Trump (2011) has shown that there is a strong preference for obscured AGNs to lie in disky and irregular galaxies (though their sample does not include CT-AGNs). Heavily obscured *radio* galaxies can be associated with spheroidal systems, but these are often hosted in clusters where interactions may drive gas to the nucleus. ESO 565–G019 is neither radio loud, nor does it lie in a cluster. There are similarities in some respects between ESO 565–G019 and the nearby FR I prototype Cen A (Israel 1998) in that both are early-type systems with dust. One important difference is that the obscuring column density of gas to the nucleus of Cen A is significantly lower and Compton thin ($N_{\rm H} \sim 10^{23}$ cm^{-2}; Risaliti 2002).

The question of the origin and abundance of dust in early-type galaxies remains to be settled. Detailed photometric analyses have revealed the presence of extended dust lanes, filaments, or disks in *most* systems with high-quality observational data (e.g., van Dokkum & Franx 1995; Tran et al. 2001). Recent *Herschel* observations also reveal that dust is prevalent in early-type galaxies (Smith et al. 2012). ESO 565–G019 is a warm infrared galaxy with a total IR luminosity $L_{\rm IR} = 10^{10.47} L_{\odot}$ and was prominently detected by *IRAS* in all its observing bands (Kewley et al. 2001; Strauss et al. 1992), showing that cool dust is present in the host on large scales. This can be seen in the broadband spectral energy distribution (SED) shown in Figure 4. Using the total IR luminosity and its known relation to star formation rate (SFR; Murphy et al. 2011, Equation (4)), we find SFR (ESO 565–G019) $\sim$ 3–4 $M_{\odot}$ yr^{-1} depending upon whether one uses the *Akari* or *IRAS* data. This SFR is a few times higher than that of the Milky Way, and about an order of magnitude larger than in typical early-type systems (Crocker et al. 2011). In order to estimate the mass of this extended cool dust component, we use Equation (1) of Smith et al. (2012) and their assumptions about the dust properties in conjunction with the observed 100 μm *IRAS* flux of ESO 565–G019. The main uncertainty is the dust temperature ($T_{\rm d}$) because the reported far-infrared fluxes do not probe beyond 90–100 μm. A $T_{\rm d} = 40$ K blackbody can describe the 60–100 μm regime well, though we caution that even cooler dust may well be present. This yields a total cool dust mass of $\sim 5 \times 10^6$ $M_{\odot}$ for ESO 565–G019, a value that lies at the upper end of the range of dust masses found by Smith et al. (2012), assuming $T_{\rm d} = 30$ K would increase the mass by a further factor of three.

But high columns of hot *nuclear* dust and associated obscuring gas in typical early-type systems remain rare. Only about 3% of BAT AGNs are hosted in ellipticals (Koss et al. 2011), with none identified as being CT thus far. Thus, confirmation of the exact morphological class of ESO 565–G019 is important. If it turns out to be of E type, then it would be the first of its kind.

5.7. Possible Triggers of Nuclear Activity

5.7.1. Interaction with ESO 565–G018

ESO 565–G019 is a member of a wide pair with ESO 565–G018 (Lauberts 1982; Reduzzi & Rampazzo 1995) separated by a projected distance of ≈17 kpc. Figure 3 shows that ESO 565–G018 appears to be elongated along their separation line. If the nuclear activity in ESO 565–G019 is a result of neighbor interaction, then this is not accompanied by significant morphological disruption of its host.

[21] ESO 138–G001 (Piconcelli et al. 2011), Mrk 3 (e.g., Awaki et al. 2008), and ESO 323–G032 (Comastri et al. 2010).

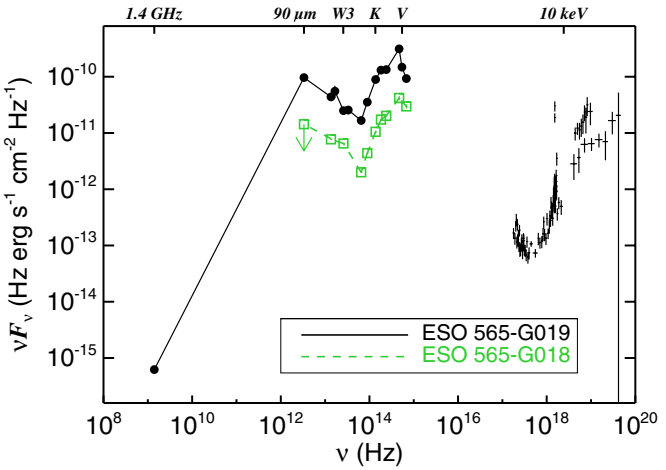

Figure 4. Broadband SED of ESO 565–G019 in black including our *Suzaku*+*Swift* X-ray unfolded model M, together with the following archival measurements: 1.4 GHz radio data from the NRAO Very Large Array sky survey (Condon et al. 1998); *Akari* 90 μm far-infrared data from Yamamura et al. (2010); *Akari* 18 and 9 μm data from Ishihara et al. (2010); 22, 12, 4.6, and 3.4 μm MIR data from the *WISE* all-sky data release (Wright et al. 2010); *Ks*-, *H*-, and *J*-band near-IR data from Two Micron All Sky Survey, as measured in $14'' \times 14''$ aperture (Skrutskie et al. 2006); *R* and *B* Cousins filter photometry from the ESO-LV survey showing R_{25} and B_{25} standard aperture measurements (Lauberts 1982); and *V*-band (V_T) data from RC3 (de Vaucouleurs et al. 1991). Data for ESO 565–G018 are shown in green. These are drawn from the same sources, where available. This source is undetected with *Akari*, and the nominal 80% completeness limit of 0.43 Jy is plotted as an upper limit at 90 μm (Yamamura et al. 2010).

(A color version of this figure is available in the online journal.)

Simulations of galaxy mergers show that pronounced star formation and nuclear activity can follow close encounters between the merging pair (e.g., Di Matteo et al. 2005). This means that ESO 565–G018 and ESO565–G019 have likely undergone at least one close passage already. We have discussed the elevated SFR in ESO 565–G019 as inferred from its high total IR luminosity. Its neighbor ESO 565–G018 is about a factor of 10 fainter in the optical and IR, and has remained undetected with both *IRAS* and *Akari* in the far-IR. Figure 4 compares the broadband SEDs of the two galaxies. So, if a close interaction is ongoing, it appears to have triggered elevated star formation in one system but not the other.

In this respect, the interaction may be similar to that of M81 and M82—the nearest galaxy pair where a close interaction has led to a well-studied nuclear starburst and pronounced morphological distortion in M82 (e.g., Gandhi et al. 2011 and references therein) but not its neighbor. A perigalactic approach of ∼21 kpc between the pair occurred about 0.5 Gyr ago (e.g., Brouillet et al. 1991), triggering a burst of star cluster formation at that time (de Grijs et al. 2001). The present starburst is associated with later nuclear infall of tidally disrupted interstellar material (e.g., O'Connell & Mangano 1978).

If the two pairs of galaxies were similar, then we may expect to find tidal signatures in the ESO 565 pair in deep multi-wavelength imaging. However, unlike M82, which is dominated by its disk, ESO 565–G019 is bulge dominated. This may well render it more resilient to interaction-induced morphological changes (see, e.g., the simulations by Mihos

& Hernquist 1994b). Conversely, one may also expect AGN activity in M82, similar to that seen in ESO 565–G019. But despite many efforts to locate ongoing accretion onto any supermassive black hole, none have been identified so far (Gandhi et al. 2011), which perhaps emphasizes the importance of supernova feedback in disrupting continuous accretion onto any AGN in M82 over the past 0.5 Gyr.

Finally, we also mention the study of Yuan et al. (2010), who investigate the co-evolution of starbursts and AGNs in a large sample of IR-selected galaxy mergers. According to their optical spectral line diagnostics, ESO 565–G019 is strongly AGN dominated ($D_{\rm AGN} = 0.8$ in their terminology). Overall, AGN dominance and total IR luminosity increase with the progression of a merger in their sample, but ESO 565–G019 is unusual in being highly AGN dominated despite its wide binary separation and moderate IR luminosity. This suggests that even if an interaction with ESO 565–G018 is ongoing, additional influences ought to be examined.

5.7.2. Past Mergers

The early-type morphological classification of ESO 565–G019 suggests that it may already be in the final stages of a past major merger, with a mature spheroid being the end product and the remnants of the merger now providing the gas that obscures and feeds the nucleus. In this scenario, however, ESO 565–G019 would not follow the now-popular merger and feedback-driven evolutionary scheme of symbiotic AGNs and galaxy growth (e.g., Hopkins et al. 2006; Sanders et al. 1988) in which energetic feedback from accretion can clear away accreting gas and results in a "dead" supermassive black hole at the nucleus. The nucleus of ESO 565–G019 is obviously surrounded by plentiful gas and growing at a radiatively efficient rate at present.

Instead, perhaps a more likely possibility is that a recent minor merger of a small system with ESO 565–G019 may have triggered enhanced nuclear activity, especially if the merger was "wet" and brought in a large amount of gas. Such mergers should be quite common, a hypothesis supported by simulations and observations, though they are not easy to identify. For instance, in simulations carried out by Mihos & Hernquist (1994a) it was found that a typical 10:1 merger of a disk system with a dwarf galaxy can briefly elevate SFRs by factors of a few, as appears to be the case for ESO 565–G019. With regard to observational evidence, Fabbiano et al. (2011) recently discovered a highly compact AGN pair in the spiral galaxy NGC 3393—thought to be the result of a minor merger in which both AGNs of the pair are hidden by CT obscuration. Simulations by Callegari et al. (2011) have shown that in minor mergers, the smaller system of the pair undergoes distinct episodes of enhanced accretion that greatly promote its growth as compared to the growth of the larger black hole. This implies that many more such minor merger pairs with both black hole components actively accreting ought to be widely detectable.

Figure 3 shows an apparent asymmetry in the nuclear regions of ESO 565–G019, which could be disruption related to minor merger activity. If so, then this would be the first minor-merger-driven RD-AGN in an early-type galaxy. A double AGN may then also be present. High angular resolution optical, X-ray, and IR imaging in the future should be able to help distinguish between the various possibilities discussed above and also shed light on the relevance of any secular processes involved in triggering the observed nuclear activity.

6. CONCLUSIONS

We have presented the first X-ray spectrum of ESO 565–G019 below 10 keV, as well as broadband X-ray spectral modeling. An RD nuclear continuum and prodigious Fe fluorescence emission have been revealed with *Suzaku*. The los obscuring column density is greater than $1.6 \times 10^{24}\,{\rm cm}^{-2}$ (90% confidence) and the Fe Kα EW with respect to the observed continuum is close to 1 keV. There is evidence of hard X-ray variability when comparing our *Suzaku* data with the long-term *Swift*/BAT average spectrum. This object is one of the few bona fide RD-AGNs known to be hosted in an early-type galaxy. Mid- and far-infrared detections point to the likely presence of massive quantities of large-scale dust and ongoing star formation in the host. The most likely scenario for triggering nuclear activity is a minor merger, though there may also be an ongoing interaction with its neighbor ESO 565–G018. Our work shows that other RD-AGNs will be uncovered in the nearby universe once the sensitivity of hard X-ray selection increases. Whether or not this population will turn out to be cosmologically significant will soon be investigated with the new generation of hard X-ray missions *NuSTAR* and *Astro-H*.

P.G. acknowledges support from JAXA and STFC (grant reference ST/J00369711). The authors thank *Suzaku* team members. K.V. thanks Y. Wadadekar and S. Barway for enlightening discussions. P.G. thanks S. F. Hönig for comments. *Swift*/BAT transient monitor data are used herein. This research has made use of the NASA/IPAC Extragalactic Database (NED), which is operated by the Jet Propulsion Laboratory, California Institute of Technology, under contract with the National Aeronautics and Space Administration. *WISE* is a project of University of California, Los Angeles, and Jet Propulsion Laboratory (JPL)/California Institute of Technology (Caltech), funded by the NASA. 2MASS is a project of the University of Massachusetts and the Infrared Processing and Analysis Center/Caltech funded by NASA and the National Science Foundation. *Akari* is a project of the Japan Aerospace Exploration Agency with the participation of the European Space Agency. The NASA/IPAC Infrared Science Archive (IRSA) operated by JPL under contract with NASA was used for querying the infrared databases. The HyperLEDA database was also useful in this work. The reviewer provided constructive criticisms that improved the paper. The Suzaku data used herein are available from the publicly open data archive at JAXA.

REFERENCES

Akylas, A., Georgakakis, A., Georgantopoulos, I., Brightman, M., & Nandra, K. 2012, A&A, 546, A98
Alexander, D. M., Bauer, F. E., Brandt, W. N., et al. 2011, ApJ, 738, 44
Alonso, M. V., Bernardi, M., da Costa, L. N., et al. 2003, AJ, 125, 2307
Armentrout, B. K., Kraemer, S. B., & Turner, T. J. 2007, ApJ, 665, 237
Arnaud, K. A. 1996, in ASP Conf. Ser. 101, Astronomical Data Analysis Software and Systems V, Vol. 5, ed. G. H. Jacoby & J. Barnes (San Francisco, CA: ASP), 17
Asmus, D., Gandhi, P., Smette, A., Hönig, S. F., & Duschl, W. J. 2011, A&A, 536, A36
Awaki, H., Anabuki, N., Fukazawa, Y., et al. 2008, PASJ, 60, 293
Ballantyne, D. R., Draper, A. R., Madsen, K. K., Rigby, J. R., & Treister, E. 2011, ApJ, 736, 56
Barthelmy, S. D., Barbier, L. M., Cummings, J. R., et al. 2005, SSRv, 120, 143
Bassani, L., Dadina, M., Maiolino, R., et al. 1999, ApJS, 121, 473
Baumgartner, W. H., Tueller, J., Markwardt, C. B., et al. 2013, ApJS, 207, 19

Blackburn, J. K. 1995, in ASP Conf. Ser. 77, Astronomical Data Analysis Software and Systems IV, ed. R. A. Shaw, H. E. Payne, & J. J. E. Hayes (San Francisco, CA: ASP), 367
Brightman, M., & Ueda, Y. 2012, MNRAS, 423, 702
Brouillet, N., Baudry, A., Combes, F., Kaufman, M., & Bash, F. 1991, A&A, 242, 35
Burlon, D., Ajello, M., Greiner, J., et al. 2011, ApJ, 728, 58
Callegari, S., Kazantzidis, S., Mayer, L., et al. 2011, ApJ, 729, 85
Cappi, M., Panessa, F., Bassani, L., et al. 2006, A&A, 446, 459
Comastri, A., Iwasawa, K., Gilli, R., et al. 2010, ApJ, 717, 787
Condon, J. J., Cotton, W. D., Greisen, E. W., et al. 1998, AJ, 115, 1693
Crocker, A. F., Bureau, M., Young, L. M., & Combes, F. 2011, MNRAS, 410, 1197
Cusumano, G., La Parola, V., Segreto, A., et al. 2010, A&A, 510, A48
Dadina, M. 2008, A&A, 485, 417
de Grijs, R., O'Connell, R. W., & Gallagher, J. S., III. 2001, AJ, 121, 768
de Vaucouleurs, G., de Vaucouleurs, A., Corwin, H. G., Jr., et al. 1991, Third Reference Catalogue of Bright Galaxies. Volume I: Explanations and References. Volume II: Data for Galaxies between 0^h and 12^h. Volume III: Data for Galaxies between 12^h and 24^h (New York: Springer)
Della Ceca, R., Severgnini, P., Caccianiga, A., et al. 2008, MmSAI, 79, 65
Di Matteo, T., Springel, V., & Hernquist, L. 2005, Natur, 433, 604
Dickey, J. M., & Lockman, F. J. 1990, ARA&A, 28, 215
Done, C., Madejski, G. M., Życki, P. T., & Greenhill, L. J. 2003, ApJ, 588, 763
Fabbiano, G., Wang, J., Elvis, M., & Risaliti, G. 2011, Natur, 477, 431
Fabian, A. C., & Iwasawa, K. 1999, MNRAS, 303, L34
Fiore, F., Grazian, A., Santini, P., et al. 2008, ApJ, 672, 94
Forman, W., Jones, C., & Tucker, W. 1985, ApJ, 293, 102
Gabor, J. M., Impey, C. D., Jahnke, K., et al. 2009, ApJ, 691, 705
Gandhi, P., Crawford, C. S., Fabian, A. C., & Johnstone, R. M. 2004, MNRAS, 348, 529
Gandhi, P., & Fabian, A. C. 2003, MNRAS, 339, 1095
Gandhi, P., Fabian, A. C., Suebsuwong, T., et al. 2007, MNRAS, 382, 1005
Gandhi, P., Horst, H., Smette, A., et al. 2009, A&A, 502, 457
Gandhi, P., Isobe, N., Birkinshaw, M., et al. 2011, PASJ, 63, 505
Gehrels, N., Chincarini, G., Giommi, P., et al. 2004, ApJ, 611, 1005
Gilli, R., Comastri, A., & Hasinger, G. 2007, A&A, 463, 79
Goulding, A. D., & Alexander, D. M. 2009, MNRAS, 398, 1165
Goulding, A. D., Alexander, D. M., Bauer, F. E., et al. 2012, ApJ, 755, 5
Guainazzi, M., & Bianchi, S. 2007, MNRAS, 374, 1290
Guainazzi, M., Matt, G., & Perola, G. C. 2005, A&A, 444, 119
Hoenig, S. F. 2013, in Proc. Torus Workshop 2012, Univ. of Texas San Antonio, 2012 December, ed. C. Packham, R. Mason, & A. Alonso-Herrero (San Antonio, TX: UTSA), arXiv:1301.1349
Hönig, S. F., Leipski, C., Antonucci, R., & Haas, M. 2011, ApJ, 736, 26
Hopkins, P. F., Hernquist, L., Cox, T. J., et al. 2006, ApJS, 163, 1
Horst, H., Gandhi, P., Smette, A., & Duschl, W. J. 2008, A&A, 479, 389
Huchra, J. P., Macri, L. M., Masters, K. L., et al. 2012, ApJS, 199, 26
Illarionov, A., Kallman, T., McCray, R., & Ross, R. 1979, ApJ, 228, 279
Ishihara, D., Onaka, T., Kataza, H., et al. 2010, A&A, 514, A1
Israel, F. P. 1998, A&ARv, 8, 237
Itoh, T., Done, C., Makishima, K., et al. 2008, PASJ, 60, 251
Iwasawa, K., Wilson, A. S., Fabian, A. C., & Young, A. J. 2003, MNRAS, 345, 369
Kewley, L. J., Heisler, C. A., Dopita, M. A., & Lumsden, S. 2001, ApJS, 132, 37
Kinkhabwala, A., Sako, M., Behar, E., et al. 2002, ApJ, 575, 732
Kokubun, M., Makishima, K., Takahashi, T., et al. 2007, PASJ, 59, 53
Konami, S., Matsushita, K., Gandhi, P., & Tamagawa, T. 2012, PASJ, 64, 117
Koss, M., Mushotzky, R., Veilleux, S., et al. 2011, ApJ, 739, 57
Koyama, K., Tsunemi, H., Dotani, T., et al. 2007, PASJ, 59, 23
Lauberts, A. 1982, ESO/Uppsala Survey of the ESO(B) Atlas (Garching: European Southern Observatory)
Levenson, N. A., Krolik, J. H., Życki, P. T., et al. 2002, ApJL, 573, L81
Madejski, G., Done, C., Życki, P. T., & Greenhill, L. 2006, ApJ, 636, 75
Magdziarz, P., & Zdziarski, A. A. 1995, MNRAS, 273, 837
Martínez-Sansigre, A., Rawlings, S., Bonfield, D. G., et al. 2007, MNRAS, 379, L6
Matsuta, K., Gandhi, P., Dotani, T., et al. 2012, ApJ, 753, 104
Matt, G. 2002, MNRAS, 337, 147
Matt, G., Brandt, W. N., & Fabian, A. C. 1996, MNRAS, 280, 823
Matt, G., Fabian, A. C., Guainazzi, M., et al. 2000, MNRAS, 318, 173
Mihos, J. C., & Hernquist, L. 1994a, ApJL, 425, L13
Mihos, J. C., & Hernquist, L. 1994b, ApJL, 431, L9
Mitsuda, K., Bautz, M., Inoue, H., et al. 2007, PASJ, 59, 1
Murphy, E. J., Condon, J. J., Schinnerer, E., et al. 2011, ApJ, 737, 67
O'Connell, R. W., & Mangano, J. J. 1978, ApJ, 221, 62
Piconcelli, E., Bianchi, S., Vignali, C., Jiménez-Bailón, E., & Fiore, F. 2011, A&A, 534, A126
Prugniel, P., & Heraudeau, P. 1998, A&AS, 128, 299
Reduzzi, L., & Rampazzo, R. 1995, ApL&C, 30, 1
Ricci, C., Walter, R., Courvoisier, T. J.-L., & Paltani, S. 2011, A&A, 532, A102
Rieke, G. H., Cutri, R. M., Black, J. H., et al. 1985, ApJ, 290, 116
Risaliti, G. 2002, A&A, 386, 379
Risaliti, G., Maiolino, R., & Salvati, M. 1999, ApJ, 522, 157
Sako, M., Kahn, S. M., Paerels, F., & Liedahl, D. A. 2000, ApJL, 543, L115
Sanders, D. B., Soifer, B. T., Elias, J. H., et al. 1988, ApJ, 325, 74
Sazonov, S., Revnivtsev, M., Krivonos, R., Churazov, E., & Sunyaev, R. 2007, A&A, 462, 57
Schommer, R. A., Caldwell, N., Wilson, A. S., et al. 1988, ApJ, 324, 154
Setti, G., & Woltjer, L. 1989, A&A, 224, L21
Severgnini, P., Caccianiga, A., & Della Ceca, R. 2012, A&A, 542, A46
Skrutskie, M. F., Cutri, R. M., Stiening, R., et al. 2006, AJ, 131, 1163
Smith, M. W. L., Gomez, H. L., Eales, S. A., et al. 2012, ApJ, 748, 123
Smith, R. K., Brickhouse, N. S., Liedahl, D. A., & Raymond, J. C. 2001, ApJL, 556, L91
Strauss, M. A., Huchra, J. P., Davis, M., et al. 1992, ApJS, 83, 29
Takahashi, T., Abe, K., Endo, M., et al. 2007, PASJ, 59, 35
Takahashi, T., Mitsuda, K., Kelley, R., et al. 2012, Proc. SPIE, 8443, 84431Z
Tran, H. D., Tsvetanov, Z., Ford, H. C., et al. 2001, AJ, 121, 2928
Treister, E., Urry, C. M., & Virani, S. 2009, ApJ, 696, 110
Trump, J. R. 2011, in Galaxy Mergers in an Evolving Universe, ed. D. B. Sanders, N. Z. Scoville, W.-H. Sun, & K. C. Xu (San Francisco, CA: ASP), arXiv:1112.3970
Tueller, J., Baumgartner, W. H., Markwardt, C. B., et al. 2010, ApJS, 186, 378
Turner, T. J., George, I. M., Nandra, K., & Mushotzky, R. F. 1997, ApJS, 113, 23
Vaghmare, K., Barway, S., & Kembhavi, A. 2013, ApJL, 767, L33
van Dokkum, P. G., & Franx, M. 1995, AJ, 110, 2027
Vasudevan, R. V., Brandt, W. N., Mushotzky, R. F., et al. 2013, ApJ, 763, 111
Vasudevan, R. V., Fabian, A. C., Gandhi, P., Winter, L. M., & Mushotzky, R. F. 2010, MNRAS, 402, 1081
Véron-Cetty, M.-P., & Véron, P. 2006, A&A, 455, 773
Wright, E. L., Eisenhardt, P. R. M., Mainzer, A. K., et al. 2010, AJ, 140, 1868
Yamamura, I., Makiuti, S., Ikeda, N., et al. 2010, yCat, 2298, 0
Yaqoob, T. 2012, MNRAS, 423, 3360
Yuan, T.-T., Kewley, L. J., & Sanders, D. B. 2010, ApJ, 709, 884